THE OBSERVATION DENSITY AND SCAN ANGLE DISTRIBUTIONS OF A SPIN-STABILIZED, PRECESSING, SCANNING SATELLITE INSTRUMENT: I. GEOMETRY.

MARC A. MURISON
U.S. Naval Observatory, 3450 Massachusetts Ave NW, Washington DC 20392
murison@aa.usno.navy.mil

January 11, 2001 D:\FAME\dynamics\ObservationDensity\Geometry.lwp

ABSTRACT

This first in a series of papers investigates the geometrical foundation of the observation density and scan angle distributions that a spin-stabilized, precessing, scanning satellite instrument generates.

Key words: FAME, Sun angle, precession cone angle, observation density, scan angle

1. INTRODUCTION

Suppose we have a distribution of stars, $f(\lambda, \beta, V)$, where β is the ecliptic latitude, λ is the ecliptic longitude, V is the visual magnitude, and f has units of stars per square degree per magnitude. In order to minimize the errors of the astrometric parameters (position, parallax, proper motion), two distributions each must be both as dense and as uniform as possible: the density of observations on the sky, and the angle at which observations are made (i.e., viewport scan direction) for any given star at a given location on the sky. We will call this latter angle the *scan angle*. The distribution of observation density and the distribution of scan angle of a spin-stabilized scanning spacecraft with n observation ports aimed perpendicularly to the spin axis, which is precessing around the nominal Sun direction, will depend on the angle (called the *Sun angle*, or, more precisely, the *precession cone angle*) between the spin axis and the nominal Sun direction, ψ; the rate of change of the precession phase φ; the rate of change of the spin phase θ; and the directions (λ, β) of the observation ports as a function of time. The latter can be characterized by the spin phase of the satellite, θ, relative, say, to the ascending node of the spacecraft equator, and the angle between observation ports, γ (called the *basic angle*). The observation density will also depend on the details of the star distribution $f(\lambda, \beta, V)$, as well as the phase of the satellite orbit around the Sun (i.e., the time of year), since the distribution of stars on the sky, roughly symmetric with respect to Galactic coordinates, is skewed with respect to ecliptic coordinates.

We choose in this study to use ecliptic coordinates, since the motion of the spacecraft spin vector, and hence the viewport direction and scan angle, are all most naturally expressed in that frame. Consideration of the effects of a nonuniform stellar density distribution $f(\lambda, \beta, V)$ is postponed to a future study. This work will concentrate on the density distribution of observations on the sky, the distribution of scan angle on the sky, and the approximate effects of inhomogeneities of these distributions on the errors of the five standard astrometric parameters (position, proper motion, and parallax).

To lowest order, the motion of the spin vector is a smooth precession around the nominal Sun direction. In actuality, the precession cone "wobbles" with respect to the Sun, as the Sun tries to drift away from the precession cone symmetry axis due to Earth's orbital motion. Solar radiation torques (acting primarily on an effectively conical but nearly flat Sun shield) counter this drift, moving the precession cone axis back towards the instantaneous direction, which is constantly changing due to orbital motion, of the Sun (e.g. Slabinsky, 1998; Reasenberg, 1999; Lim, 2000). The result is to cause the precession cone symmetry axis to track the Sun direction in an epicyclic fashion. Here we ignore this and other, smaller, perturbations on the gross motions of the spacecraft spin vector.

In previous work, Reasenberg (1997) considered the distributions of observation density and of scan angle, averaging over ecliptic longitude. Based on this initial foray into the problem, he concluded from histograms of the observation density and scan angle (averaged over ecliptic longitude) that variation of the precession cone angle (in the range 35 to 55 degrees) does not appear to cause drastic changes in the distributions. The corresponding implication is that the precession cone angle may perhaps be chosen in the range 35-55 degrees without large effects on mission accuracies, though that of course remains to be addressed explicitly.

As part of a mission simulation (duration: 0.5 yr, number of stars: 450) for HIPPARCOS, Høyer et al. (1981) included a very brief look at the relative changes in full-sky-averaged mission accuracies of positions in ecliptic coordinates for three values (20°, 30°, 40°) of the precession cone angle (which Høyer et al. referred to as the "revolving angle"). The Høyer simulation consisted of statistically generated observations coupled with nonlinear weighted least squares parameter estimation. They found ratios of the sky-averaged mean errors in β to be 1.13 : 1.00 : 0.97, and of the sky-averaged mean errors in λ to be 1.70 : 1.00 : 0.76, at the three respective values of precession cone angle. As will be shown in the present study, averaging over the full sky masks important effects and is therefore at best a questionable metric of the two distributions. In an Appendix to their paper, Høyer et al. also performed an analytical analysis in which they averaged over scan angle and

spin phase (designated θ in the present study). Comparison with their simulation results showed a "marked" (their word) difference (0.92 : 1.00 : 1.09 and 1.20 : 1.00 : 0.90, respectively), which they were unable to explain. The difference in behavior between the Høyer et al. analytical approach and their numerical simulations is probably due to the averaging they performed in order to make the analytical problem tractable. Their numerical simulations did not incorporate such averaging. In any case, the simulation results are clear: one does better with larger Sun angles, at least when averaging the errors over the entire sky. Neither Reasenberg nor Høyer et al. considered the effects on the two distributions of changing the precession rate.

In this series of papers, I examine the distributions in greater depth and in more quantitative detail, as well as consider the effects of changing both the precession cone angle and the precession rate, all without performing any statistical averaging of quantities. This first paper in the series reviews the relevant geometry of the problem. We specify the viewport coordinates in terms of ecliptic coordinates, and we determine the scan angle as a function of the precession cone angle and ecliptic coordinates. We also specify the spin and precession phase angles as functions of the precession cone angle and ecliptic coordinates. These will be useful throughout the rest of the study. In the second paper, we look in detail at the in-scan, cross-scan, and field rotation rates as functions of position on the sky, in order to understand the form and behavior of the distributions found in the simulations of the third and fourth papers. The third paper presents the distributions of both observation density and scan angle that result from observation time series. The purpose is to develop an understanding of the characteristics of the distributions and of their behavior with changes in precession cone angle and precession rate. The fourth paper addresses via simulated observations the effects of the distribution inhomogeneities on mission accuracies of the classical astrometric parameters. The main results of this study are contained in the third and especially the fourth papers.

This work is broken up into four papers for the sake of convenience, for two reasons. First, it provides some relief to the reader, since the divisions fall along natural breaks in the development. Second, much of the computational work is performed in the Maple computer algebra system environment, with the consequence that computer hardware limitations make it impossible to contain the entire work in a single Maple document. The four papers are not stand-alone in nature but are meant to be read in sequence.

2. SPHERICAL GEOMETRY OF THE PROBLEM

2.1. Transformation between External and Body Frames

Consider two Cartesian frames of reference: (1) a frame $[x, y, z]$ fixed to the spacecraft body, with the z axis along the spacecraft symmetry axis (i.e., the spin axis) and the y axis piercing the focal plane of viewport 1, and (2) an external frame $[X, Y, Z]$. The external frame need not be inertial. The two frames can be related to each other via Euler angles, one convenient set of which is shown in Figure 1. Viewport 2 trails viewport 1 by an angle, γ, the so-called *basic angle*.

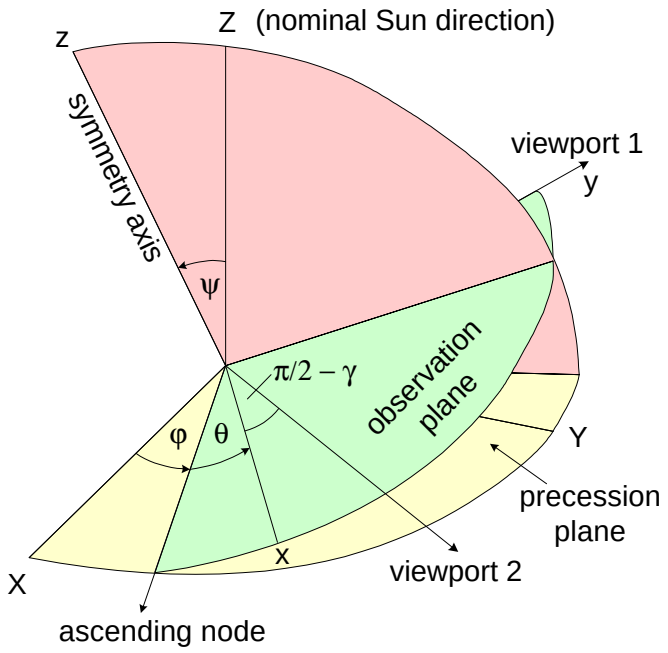

Figure 1 — The body frame $[x, y, z]$ and the external frame $[X, Y, Z]$, connected by the Euler angles $[\theta, \psi, \varphi]$. The "fast" angle, or spin phase, is θ; the precession phase is φ; and the precession cone angle, or nominal Sun angle, is ψ. The two viewports are separated by the "basic angle", γ.

To transform from the external frame to the body frame, first rotate around the Z axis by φ, then around X' by ψ (the inclination angle, *aka* the Sun angle or, more accurately, the precession cone angle), then around Z'' by θ, the "fast" Euler angle. One may easily develop the resulting coordinate transformation matrix, which we do here explicitly for reference.

Rotate the external frame coordinates ccw around the Z axis (cf. Figure 1):

$$R_Z(\varphi) = \begin{bmatrix} \cos\varphi & \sin\varphi & 0 \\ -\sin\varphi & \cos\varphi & 0 \\ 0 & 0 & 1 \end{bmatrix} \tag{1}$$

Next, a matrix to rotate ccw around the X' axis:

$$R_X(\psi) = \begin{bmatrix} 1 & 0 & 0 \\ 0 & \cos\psi & \sin\psi \\ 0 & -\sin\psi & \cos\psi \end{bmatrix} \tag{2}$$

Then a matrix to rotate ccw around the Z'' axis:

$$R_Z(\theta) = \begin{bmatrix} \cos\theta & \sin\theta & 0 \\ -\sin\theta & \cos\theta & 0 \\ 0 & 0 & 1 \end{bmatrix} \tag{3}$$

Now combine the rotations in this order into a single rotation matrix. The resulting coordinate transformation is

$$\begin{bmatrix} x \\ y \\ z \end{bmatrix} = R(\varphi, \psi, \theta) \begin{bmatrix} X \\ Y \\ Z \end{bmatrix} \tag{4}$$

where

$$R(\varphi,\psi,\theta)=\begin{bmatrix}\cos\theta\cos\varphi-\sin\theta\sin\varphi\cos\psi & \cos\theta\sin\varphi+\sin\theta\cos\varphi\cos\psi & \sin\theta\sin\psi\\ -\sin\theta\cos\varphi-\cos\theta\sin\varphi\cos\psi & -\sin\theta\sin\varphi+\cos\theta\cos\varphi\cos\psi & \cos\theta\sin\psi\\ \sin\varphi\sin\psi & -\cos\varphi\sin\psi & \cos\psi\end{bmatrix} \tag{5}$$

Using eqs. (4) and (5), we can transform coordinates from the external frame $[X,Y,Z]$ to the body frame $[x,y,z]$ and *vice versa*. We can rotate the observing plane so that the y axis pierces viewport 2 instead of viewport 1 by substituting $\theta-\gamma$ in place of θ. Transformations between the external frame and other external frames (e.g., equatorial coordinates, galactic coordinates, and so on) can be similarly constructed.

2.2. Viewport Ecliptic Coordinates and the Scan Angle as Functions of the Euler Angles

We are interested in the distribution on the sky of observations taken through the spacecraft viewports, as well as the distribution of the scan angle q. Since the Sun plays a pervasive role throughout, rotating ecliptic coordinates such that the nominal Sun direction is along the Z axis are a natural choice for the external frame.[1]

In Figure 2, (λ,β) are the ecliptic longitude and latitude of the two spacecraft viewports, and $\lambda_\odot$ is the ecliptic longitude of the Sun. In this figure the spacecraft spin vector points below the XZ plane. Elsewhere (Murison, 2000a), I show how the large spherical triangle composed of smaller triangles A and B yield the ecliptic coordinates of the leading viewport,

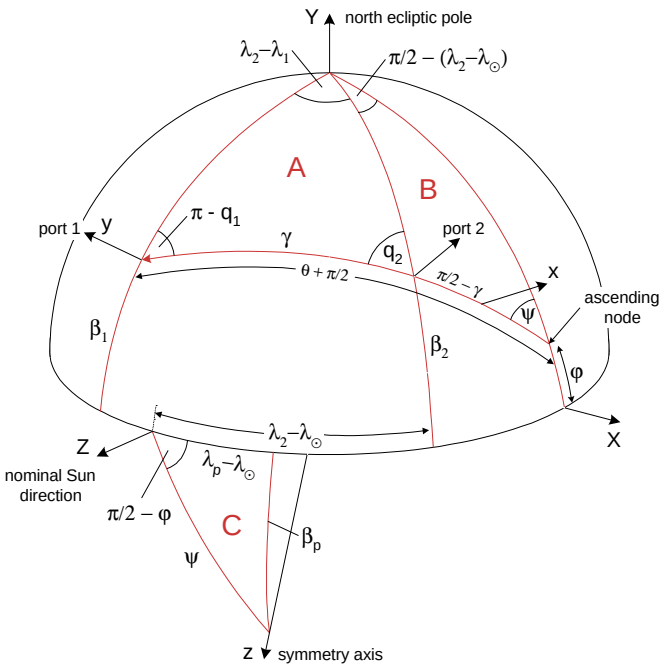

Figure 2 — Spherical geometry of the two viewports and the symmetry axis spin vector, in the ecliptic coordinate frame

$$\sin\beta_1=-\sin\varphi\sin\theta+\cos\varphi\cos\theta\cos\psi \tag{6}$$

$$\cos\lambda_1=\frac{\cos\theta\sin\psi\cos\lambda_\odot+(\sin\theta\cos\varphi+\cos\theta\sin\varphi\cos\psi)\sin\lambda_\odot}{\sqrt{1-(\cos\varphi\cos\theta\cos\psi-\sin\varphi\sin\theta)^2}} \tag{7}$$

$$\sin\lambda_1=\frac{\cos\theta\sin\psi\sin\lambda_\odot-(\sin\theta\cos\varphi+\cos\theta\sin\varphi\cos\psi)\cos\lambda_\odot}{\sqrt{1-(\cos\varphi\cos\theta\cos\psi-\sin\varphi\sin\theta)^2}} \tag{8}$$

where $\lambda_\odot$ is the ecliptic longitude of the Sun, and (θ,ψ,φ) are Euler angles connecting the spacecraft body frame to the ecliptic frame. These Euler angles are defined in Figure 1, as well as in Murison (2000a). For the remainder of section 2, we drop the explicit subscript designation of viewport 1 and write λ,β for notational simplicity.

The distribution of ecliptic coordinates (λ,β) of the viewports on the sky resulting from a sequential series of observations is only one part of the story. The other crucial quantity is the distribution of the auxiliary angle q (often called the parallactic angle) in spherical triangle A in Figure 2. This is the angle of the instantaneous scan direction with respect to a meridian passing through the ecliptic north pole and a star with coordinates (λ,β). We shall call this angle the *scan angle*. From the large spherical triangle composed of the triangles A and B, we write (referring to q_1)

$$\sin\phi=-\sin\beta\sin\theta-\cos\beta\cos\theta\cos q \tag{9}$$

$$\cos\beta\sin q=\cos\phi\sin\psi \tag{10}$$

Hence, using (6), we obtain the result

$$\cos q=-\frac{(\cos\phi\cos\theta\cos\psi-\sin\phi\sin\theta)\sin\theta+\sin\phi}{\sqrt{1-(\cos\phi\cos\theta\cos\psi-\sin\phi\sin\theta)^2}\ \sin\theta} \tag{11}$$

$$\sin q=\frac{\cos\phi\sin\psi}{\sqrt{1-(\cos\phi\cos\theta\cos\psi-\sin\phi\sin\theta)^2}} \tag{12}$$

Notice that the scan angle q is independent of the Sun's longitude, $\lambda_\odot$. The distribution of q as a function of spin phase θ and precession phase φ is therefore static (we are ignoring variations of the precession cone angle ψ).

2.3. Scan Angle as a Function of Precession Cone Angle and Ecliptic Coordinates

From the large spherical triangle A+B, we write two more relations:

$$\sin q\cos\theta=\cos(\lambda-\lambda_\odot)\cos\phi \tag{13}$$

[1] The external frame Z axis points towards the nominal direction of the Sun. It is more accurate to say that the Z axis is coincident with the axis about which the spacecraft spin axis precesses. We will call this the "precession cone axis", or the precession axis. Due to the orbital motion of the Earth, the Sun will move away from the precession axis direction. But the resulting solar radiation torque imbalance acts to cause the precession axis to try and follow the Sun. We call this mechanism "Sun tracking". The net effect is, to lowest order, a guiding center motion: the spin axis circulates around the precession axis (the guiding center), which in turn is slowly moving to follow the Sun. Hence, the angle between the instantaneous direction of the Sun and the spin axis (the instantaneous Sun angle) will vary with an amplitude of several degrees (in the case of FAME), but the precession cone angle ψ will remain relatively constant.

$$-\sin\theta = \sin\beta\sin\phi + \cos\beta\cos\phi\sin(\lambda-\lambda_\odot) \quad (14)$$

Equations (6), (9), (10), (13), and (14) are a set of five equations in five variables. These are not completely independent, since eqs. (10) and (13) from the law of sines have two sides and two angles in common with the other three equations from the law of cosines.

Eliminate θ and φ from the five equations to obtain the reduced set

$$[\sin^2(\lambda-\lambda_\odot) - \cos^2(\lambda-\lambda_\odot)\sin^2\beta]\sin^2 q - 2\sin\beta\cos(\lambda-\lambda_\odot)\sin(\lambda-\lambda_\odot)\cos q\sin q - \sin^2\psi + \cos^2(\lambda-\lambda_\odot) = 0 \quad (15)$$

and

$$\{[\cos^2(\lambda-\lambda_\odot) - \sin^2(\lambda-\lambda_\odot)]\sin^2 q + \sin^2\psi - \cos^2(\lambda-\lambda_\odot)\}\sin\beta - [\cos(\lambda-\lambda_\odot)\cos\psi\cos^2\beta - \cos(\lambda-\lambda_\odot)\sin(\lambda-\lambda_\odot)(1+\sin^2\beta)\cos q]\sin q = 0 \quad (16)$$

Solving (15) and (16), we can write q as a function of position on the sky (λ,β), the precession cone angle ψ, and the solar longitude $\lambda_\odot$. We obtain

$$\sin q = Q \quad (17)$$

$$\cos q = \frac{[\sin^2(\lambda-\lambda_\odot) - \cos^2(\lambda-\lambda_\odot)\sin^2\beta]\cos\psi}{\sin(\lambda-\lambda_\odot)[1-\cos^2(\lambda-\lambda_\odot)\cos^2\beta]} + \frac{[\cos^2(\lambda-\lambda_\odot) - \sin^2\psi]\cos(\lambda-\lambda_\odot)\sin\beta}{Q\sin(\lambda-\lambda_\odot)[1-\cos^2(\lambda-\lambda_\odot)\cos^2\beta]} \quad (18)$$

where Q is the pair of quadratic solutions

$$Q = \frac{\cos(\lambda-\lambda_\odot)\cos\psi\sin\beta}{1-\cos^2(\lambda-\lambda_\odot)\cos^2\beta} \pm \frac{|\sin(\lambda-\lambda_\odot)|\sqrt{\sin^2\psi - \cos^2(\lambda-\lambda_\odot)\cos^2\beta}}{1-\cos^2(\lambda-\lambda_\odot)\cos^2\beta} \quad (19)$$

We see that, given a star at a position $(\lambda-\lambda_\odot,\beta)$ relative to the Sun, then for a precession cone angle ψ one can vary θ and φ until the star is in the field of view of viewport 1 (and likewise for viewport 2). This will in general occur for two values of (θ,φ), with two corresponding values of scan angle q. We are now in a position to specify the scan angle as a function of position on the sky, for a given precession cone angle and solar longitude.

The actual scan angle as defined is not quite the angle q that we've determined in eqs. (17)-(19). In addition to motion of the viewport across the sky due to the fast Euler angle rate $d\theta/dt$, there is a small motion due to the precession $d\varphi/dt$, and even smaller motions due to the orbit of the Earth, $d\lambda_\odot/dt$, and to perturbations in the precession cone angle, $d\psi/dt$. The largest of these, $d\varphi/dt$, causes the angular velocity vector in the spacecraft body frame to circle the spacecraft symmetry axis with a period equal to the precession period and an angular radius r determined from simple geometry by $\tan r = \frac{d\varphi/dt}{d\theta/dt}\sin\psi$. However, for a precession period in the range 20-30 days, a precession cone angle $\psi = 45$ deg, and a spin period of 40 minutes, the angular radius of the angular velocity vector from the symmetry axis spans 135-203 arc seconds; this is the dominant error of approximating the actual scan angle with q as determined from eqs. (17)-(19). Hence, for purposes of determining distributions of the scan angle, this and smaller terms are ignorable at a level of 10^{-4}, and our "scan angle" q is quite suitable.

For each set of values ψ and $\lambda_\odot$, there will be a region of the sky that is visible, corresponding to a 2π range of the precession and spin phase angles. The boundaries of this allowed region are determined by the locations where the square root term in Q becomes imaginary. There are two resulting inaccessible "holes" in the Sun and anti-Sun directions, corresponding to the boundaries of the precession cone. The angular radius of the holes, from simple geometry, is $\frac{\pi}{2}-\psi$, which may also be seen by setting $\lambda=\lambda_\odot$ in $\sin^2\psi - \cos^2(\lambda-\lambda_\odot)\cos^2\beta$ from the square root term, leaving $\frac{\pi}{2}-\beta = \pm\psi$.

Figure 3 shows, on a sinusoidal projection of the sky, the value of the square root term as a function of β and $\Delta\lambda = \lambda-\lambda_\odot$, for $\psi = \frac{\pi}{4}$, and with black representing zero. The red circles are the boundaries of the precession cone holes.

The precession cone holes occupy a solid angle that is a function of the precession cone angle. Consider an infinitesimal solid angle element $d\Omega = \sin u\, du\, d\varphi$, where $u = \frac{\pi}{2}-\psi$ is the polar angle. Integrating over $\varphi = 0..2\pi$ and $u = 0..\frac{\pi}{2}-\psi$, we obtain the solid angle occupied by the two holes,

$$\frac{\Omega_{holes}}{4\pi} = 1-\sin\psi \quad (20)$$

Figure 4 shows the fraction of the sky occupied by the two precession cone holes as the precession cone angle varies between 36° and 54°.

Figure 5 illustrates the scan angle as a function of ecliptic latitude and difference in ecliptic longitude from that of the Sun, for a precession cone angle of 45 degrees. Again, a sinusoidal map projection in $(\Delta\lambda,\beta)$ is used. The blue and yellow surfaces correspond to the two solutions represented by eqs.

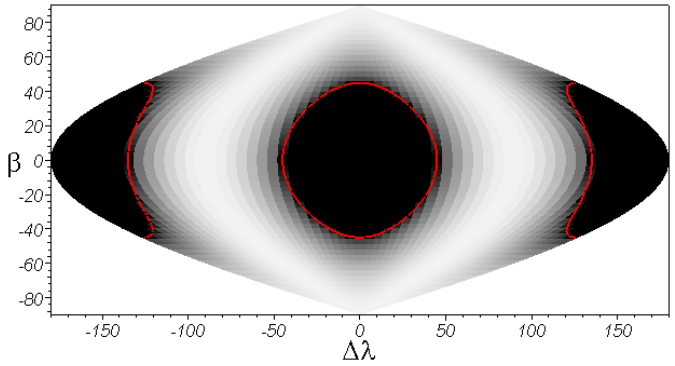

Figure 3 — Square root term of Q as a function of position on the sky. Black regions correspond to precession cone holes, the boundaries of which are indicated by the red curves. Map projection is a sinusoidal equal-area projection (Murison, 2000b).

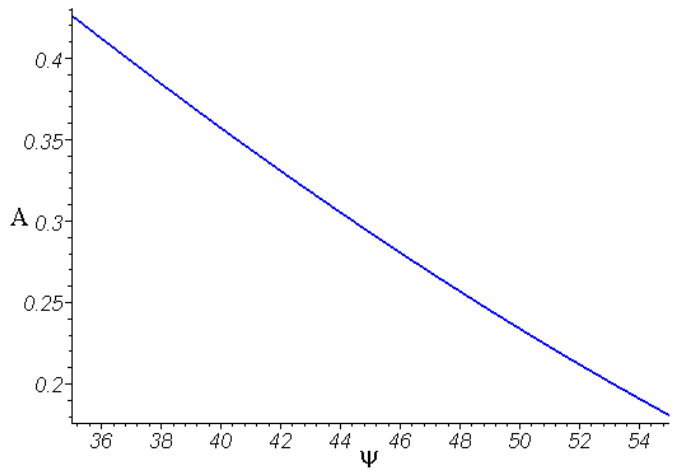

Figure 4 — Areal fraction of the sky occupied by the precession cone holes, as a function of precession cone angle in degrees.

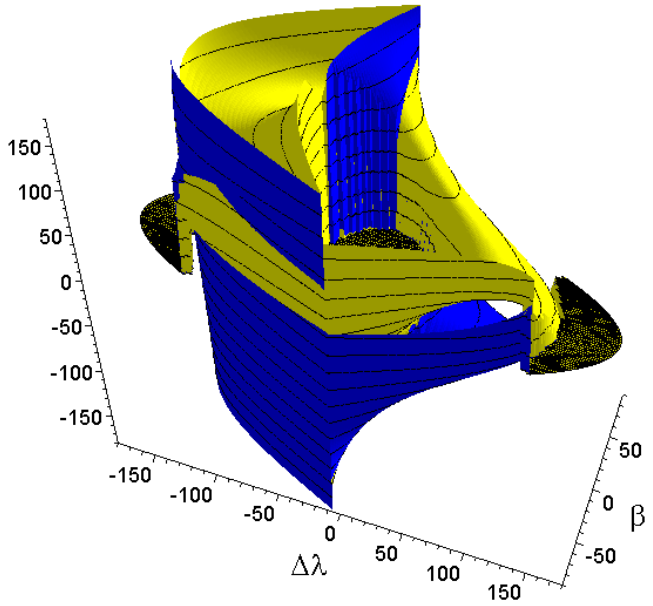

Figure 5 — Scan angle as a function of position on the sky. Map projection is a sinusoidal equal-area projection (Murison, 2000b).

(17)-(19). The holes due to the precession cone in the Sun and anti-Sun directions, shown in black, are readily apparent. The *faux* discontinuities near $\Delta\lambda \simeq \pm 130$ deg and $\Delta\lambda \simeq \pm 40$ deg are merely due to wrapping of q from -180 to 180 degrees. There are real discontinuities at $\Delta\lambda = 0, \pi$. As seen from eq. (19), the two solutions become identical at the discontinuities (note in the Figure the continuation of contour lines across the discontinuities). Hence, the surfaces match across the discontinuities to produce two continuous smoothly deformed sheets (except precisely at the infinitesimal discontinuities). The effect of decreasing the precession cone angle is to increase the radius of the precession cone holes by the same amount and to increase the fraction of the sky covered by the holes according to eq. (20).

2.4. Spin and Precession Phase as Functions of Precession Cone Angle and Ecliptic Coordinates

For reference, it will be useful to express θ and φ as functions of position on the sky (ecliptic coordinates) and of the precession cone angle ψ. Eqs. (6) and (14) are independent of the scan angle q. A third equation that does not explicitly involve q is

$$\cos\theta \sin\psi = \cos(\lambda - \lambda_\odot)\cos\beta \tag{21}$$

This equation follows directly from the triangle A+B, or it may be derived by eliminating q from eqs. (10) and (13). We therefore have the three independent equations (6), (14), and (21).

To solve for the four quantities $\sin\theta$, $\cos\theta$, $\sin\varphi$, and $\cos\varphi$, we need four independent equations. Fortunately, we can make use of the identity $\sin^2 + \cos^2 = 1$ as follows. Substitute (14) into (6) to get

$$\cos\theta = \frac{\sin\beta\cos\phi - \sin(\lambda - \lambda_\odot)\cos\beta\sin\phi}{\cos\psi} \tag{22}$$

Substitute (22) into (21) to obtain the equation

$$[\sin\beta\cos\phi - \sin(\lambda - \lambda_\odot)\cos\beta\sin\phi]\sin\psi = \cos(\lambda - \lambda_\odot)\cos\beta\cos\psi \tag{23}$$

which is independent of θ. Now substitute (21) into (6), getting

$$\sin\theta = \frac{\cos\phi\cos\psi\cos(\lambda - \lambda_\odot)\cos\beta - \sin\psi\sin\beta}{\sin\phi\sin\psi} \tag{24}$$

Plug this back into (14) to get the equation

$$\sin\psi\sin\beta - \cos\phi\cos\psi\cos(\lambda - \lambda_\odot)\cos\beta = [\sin\phi\sin\beta + \cos\phi\sin(\lambda - \lambda_\odot)\cos\beta]\sin\phi\sin\psi \tag{25}$$

which is also independent of θ. Eqs. (23) and (25) may now be solved for $\sin\varphi$ and $\cos\varphi$. From (23),

$$\sin\phi = \frac{\sin\beta\cos\phi}{\sin(\lambda - \lambda_\odot)\cos\beta} - \frac{\cos(\lambda - \lambda_\odot)\cos\psi}{\sin(\lambda - \lambda_\odot)\sin\psi} \tag{26}$$

Then (25) becomes

$$2\frac{\cos(\lambda - \lambda_\odot)\cos\phi\cos\psi\sin\beta}{\sin^2(\lambda - \lambda_\odot)\cos\beta} - \left[1 + \frac{\sin^2\beta}{\sin^2(\lambda - \lambda_\odot)\cos^2\beta}\right]\sin\psi\cos^2\phi - \frac{\cos^2(\lambda - \lambda_\odot)\cos^2\psi}{\sin^2(\lambda - \lambda_\odot)\sin\psi} + \sin\psi = 0 \tag{27}$$

which has the solutions

$$\cos\phi = \frac{\cos(\lambda - \lambda_\odot)\cos\psi\sin\beta\cos\beta}{[1 - \cos^2(\lambda - \lambda_\odot)\cos^2\beta]\sin\psi} \pm \frac{|\sin(\lambda - \lambda_\odot)|\sqrt{\sin^2\psi - \cos^2(\lambda - \lambda_\odot)\cos^2\beta}\ \cos\beta}{[1 - \cos^2(\lambda - \lambda_\odot)\cos^2\beta]\sin\psi} \tag{28}$$

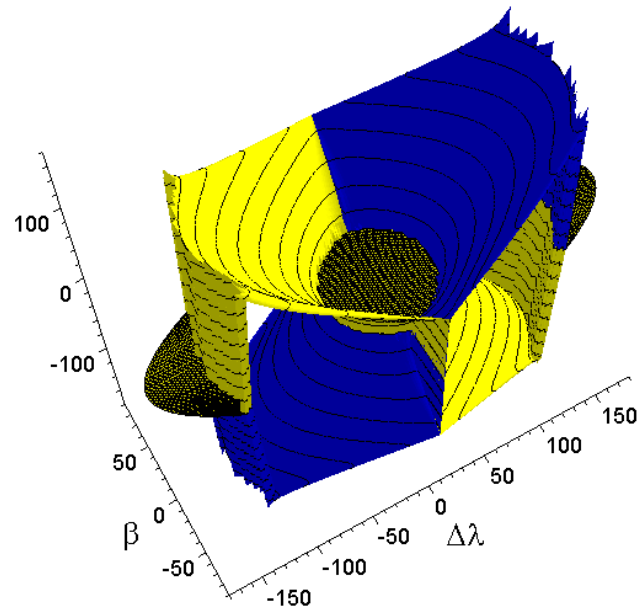

Figure 6 — Spin phase angle as a function of position on the sky. Map projection is a sinusoidal equal-area projection (Murison, 2000b).

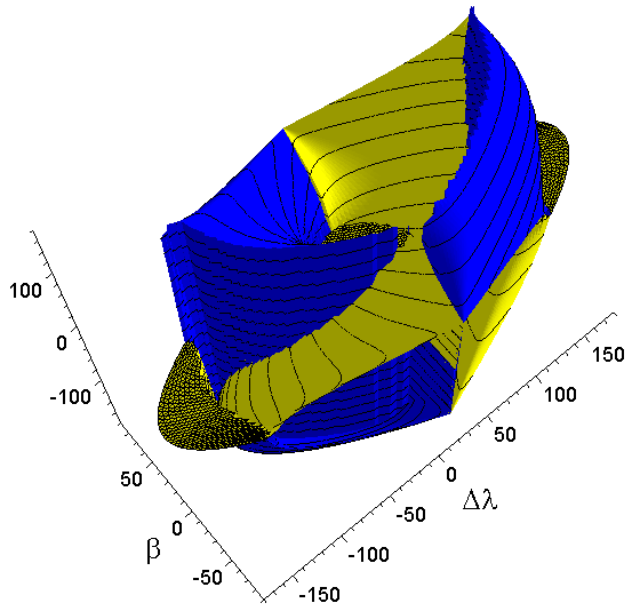

Figure 7 — Precession phase angle as a function of position on the sky. Map projection is a sinusoidal equal-area projection (Murison, 2000b).

Recalling eq. (19), we write this as

$$\cos\phi = \frac{Q\cos\beta}{\sin\psi} \tag{29}$$

Then eq. (26) becomes

$$\sin\phi = \frac{Q\sin\beta - \cos(\lambda-\lambda_\odot)\cos\psi}{\sin(\lambda-\lambda_\odot)\sin\psi} \tag{30}$$

Eqs. (29) and (30) give $\cos\varphi$ and $\sin\varphi$ as functions only of ecliptic coordinates and the precession cone angle.

Finally, substituting (29) and (30) into (22) and (24), we obtain $\cos\theta$ and $\sin\theta$ as functions of ecliptic coordinates and the precession cone angle:

$$\cos\theta = \frac{\cos(\lambda-\lambda_\odot)\cos\beta}{\sin\psi} \tag{31}$$

$$\sin\theta = \frac{[Q\cos^2\beta\cos(\lambda-\lambda_\odot)\cos\psi - \sin^2\psi\sin\beta]\sin(\lambda-\lambda_\odot)}{[Q\sin\beta - \cos(\lambda-\lambda_\odot)\cos\psi]\sin\psi} \tag{32}$$

Due to Q being multivalued, θ and φ will also exhibit precession cone holes.

Figure 6 shows θ as a function of ecliptic coordinates, while Figure 7 shows φ. As with the scan angle, the two solution surfaces for both θ and φ smoothly join at the individual surface discontinuities.

3. RESULTS FOR VIEWPORT 2

In this section we state for reference the results for viewport 2 explicitly. As previously mentioned, for viewport 2 we rotate the observing plane by the basic angle γ, so that the body frame y axis pierces viewport 2. Hence, we need only substitute $\theta-\gamma$ in place of θ in the viewport 1 equations. The ecliptic coordinates of the second (trailing) viewport are (Murison, 2000a)

$$\sin\beta_2 = -\sin\varphi\sin(\theta-\gamma) + \cos\varphi\cos(\theta-\gamma)\cos\psi \tag{33}$$

$$\cos\lambda_2 = \frac{\cos(\theta-\gamma)\sin\psi\cos\lambda_\odot}{\sqrt{1-[\cos\varphi\cos(\theta-\gamma)\cos\psi - \sin\varphi\sin(\theta-\gamma)]^2}} + \frac{[\sin(\theta-\gamma)\cos\varphi + \cos(\theta-\gamma)\sin\varphi\cos\psi]\sin\lambda_\odot}{\sqrt{1-[\cos\varphi\cos(\theta-\gamma)\cos\psi - \sin\varphi\sin(\theta-\gamma)]^2}} \tag{34}$$

$$\sin\lambda_2 = \frac{\sin(\theta-\gamma)\sin\psi\sin\lambda_\odot}{\sqrt{1-[\cos\varphi\cos(\theta-\gamma)\cos\psi - \sin\varphi\sin(\theta-\gamma)]^2}} + \frac{[\cos\psi\sin(\theta-\gamma)\sin\phi - \cos(\theta-\gamma)\cos\phi]\cos\lambda_\odot}{\sqrt{1-[\cos\varphi\cos(\theta-\gamma)\cos\psi - \sin\varphi\sin(\theta-\gamma)]^2}} \tag{35}$$

Equations (11) and (12) become

$$\cos q_2 = \frac{[\sin\phi\cos(\theta-\gamma) + \cos\phi\sin(\theta-\gamma)\cos\psi]\cos(\theta-\gamma) - \sin\phi}{\sqrt{1-(\sin\phi\cos(\theta-\gamma) + \cos\phi\sin(\theta-\gamma)\cos\psi)^2}\ \sin(\theta-\gamma)} \tag{36}$$

$$\sin q_2 = \frac{\cos\phi\sin\psi}{\sqrt{1-(\sin\phi\cos(\theta-\gamma) + \cos\phi\sin(\theta-\gamma)\cos\psi)^2}} \tag{37}$$

Finally, eqs. (17)-(19) become

$$\sin q_2 = Q_2 \tag{38}$$

$$\cos q_2 = \frac{[\sin^2(\lambda_2-\lambda_\odot) - \cos^2(\lambda_2-\lambda_\odot)\sin^2\beta_2]\cos\psi}{\sin(\lambda_2-\lambda_\odot)[1-\cos^2(\lambda_2-\lambda_\odot)\cos^2\beta_2]} + \frac{[\cos^2(\lambda_2-\lambda_\odot) - \sin^2\psi]\cos(\lambda_2-\lambda_\odot)\sin\beta_2}{Q_2\sin(\lambda_2-\lambda_\odot)[1-\cos^2(\lambda_2-\lambda_\odot)\cos^2\beta_2]} \tag{39}$$

$$Q_2 = \frac{\cos(\lambda_2-\lambda_\odot)\cos\psi\sin\beta_2}{1-\cos^2(\lambda_2-\lambda_\odot)\cos^2\beta_2} \pm \frac{|\sin(\lambda_2-\lambda_\odot)|\sqrt{\sin^2\psi-\cos^2(\lambda_2-\lambda_\odot)\cos^2\beta_2}}{1-\cos^2(\lambda_2-\lambda_\odot)\cos^2\beta_2} \quad (40)$$

4. CONCLUSIONS

Conclusions resulting from work presented in this paper may be summarized as follows:

- The scan angle and the ecliptic coordinates of the spacecraft viewports are easily expressed as functions of the spacecraft attitude, as realized in the form of Euler angles that connect the spacecraft coordinate frame to the external ecliptic frame. These functions are not terribly complicated, but neither are they trivial.
- The scan angle can be written as a function only of ecliptic coordinates, the ecliptic longitude of the Sun, and the precession cone angle. A characteristic of the solution is that it is multivalued. Specifically, there are in general two solution surfaces, corresponding to two attitude configurations that yield two scan angle values at the same location on the sky (in a frame rotating such that the Sun appears fixed on the sky).
- A pair of quadratic solution terms identified in the development of the scan angle as a function of ecliptic coordinates is found to be a common factor in all of the interesting coordinate transformations considered here. Two underlying themes result, both of which have an impact on the observation density and scan angle distributions. First, the solution surfaces that appear throughout the development contain discontinuities, and the separate surfaces join smoothly at those discontinuities. That is, a bug crawling on one solution surface and encountering a discontinuity can smoothly step across the discontinuity onto the other solution surface, as required by the physical problem. Second, the instantaneous Sun and anti-Sun directions are surrounded by precession cone "holes", inside the boundaries of which the quadratic solution terms become imaginary. These holes owe their existence to the simple geometric facts that 1) the spacecraft spin axis precesses around the nominal Sun and anti-Sun directions and 2) the viewport directions are perpendicular to the spin axis. The behavior of the quadratic solution terms is just the mathematical manifestation of these geometric facts. Not unexpectedly, the existence of the precession cone holes plays a fundamental role in the observation density and scan angle distributions. Illustrations of the solution surfaces render the surface topology and their physical origins clear.
- The precession cone hole radius is equal to $\frac{\pi}{2}-\psi$, where ψ is the precession cone angle. The smaller the precession cone angle, the larger the expected effects of the holes on the distributions. The fraction of the sky occupied by the two holes is $1-\sin\psi$.
- Finally, the spin and precession phase angles are expressed as functions of ecliptic coordinates, ecliptic longitude of the Sun, and precession cone angle. These equations are useful in simulations which will be presented in subsequent papers in this series (Murison, 2000c-e). The corresponding "surfaces" are also shown; they exhibit the topology determined by the underlying quadratic solution factors.

REFERENCES

Høyer, P., Poder, K., Lindegren, L., and Høg, E., 1981, "Derivation of Positions and Parallaxes from Simulated Observations with a Scanning Astrometry Satellite", *Astron. Astrophys.* **101**, 228.

Lim, T., 2000, private communication.

Murison, M.A., 2000a, "Ecliptic Coordinates of the FAME Viewports and Symmetry Axis", Astronomical Applications Department Technical Note AA2000-04, http://aa.usno.navy.mil/about/internal/TechNotes.html, also available directly at the URL http://aa.usno.navy.mil/Murison/Maple/EclipticCoords/EclipticCoords.pdf, and at the FAME web site as FTM2000-07 in the FAME Technical Memorandum series.

Murison, M.A., 2000b, "Characteristics of Selected Map Projections", Astronomical Applications Department Technical Note AA2000-05, http://aa.usno.navy.mil/about/internal/TechNotes.html, also available directly at the URL http://aa.usno.navy.mil/murison/Maple/MapProjections/MapProjections.pdf, and at the FAME web site as FTM2000-08 in the FAME Technical Memorandum series.

Murison, M.A., 2000c (Paper 2), "The Observation Density and Scan Angle Distributions of a Spin-Stabilized, Precessing, Scanning Satellite Instrument: II. Scan, Cross-Scan, and Field Rotation Rates", in preparation.

Murison, M.A., 2000d (Paper 3), "The Observation Density and Scan Angle Distributions of a Spin-Stabilized, Precessing, Scanning Satellite Instrument: III. Distributions from Simulated Observations", in preparation.

Murison, M.A., 2000e (Paper 4), "The Observation Density and Scan Angle Distributions of a Spin-Stabilized, Precessing, Scanning Satellite Instrument: IV. Simulated Observations on an Equal-Area Grid", in preparation.

Reasenberg, R.D., 1997, "Observation density over the sky with the HIPPARCOS observing scheme", FAME Technical Memorandum FTM97-07.

Reasenberg, R.D., 1999, "Precession of the FAME Spacecraft", FAME Technical Memorandum FTM99-04.

Slabinsky, V., 1998, notes summarizing results obtained in the 1970s, provided via private communication.